energies

MDPI

Article

Analysis of the Primary Constraint Conditions of an Efficient Photovoltaic-Thermoelectric Hybrid System

Guiqiang Li [1,*], Xiao Chen [2] and Yi Jin [3,*]

1 Department of Thermal Science and Energy Engineering, University of Science and Technology of China, 96 Jinzhai·Road, Hefei 230026, China
2 State Key Laboratory of Fire Science, University of Science and Technology of China, 96 Jinzhai Road, Hefei 230026, China; summercx@mail.ustc.edu.cn
3 Department of Precision Machinery and Precision Instrumentation, University of Science and Technology of China, Hefei 230026, China
* Correspondences: ligq@mail.ustc.edu.cn (G.L.); jinyi08@ustc.edu.cn (Y.J.); Tel./Fax: +86-551-63603512

Academic Editors: Senthilarasu Sundaram and Tapas Mallick
Received: 27 October 2016; Accepted: 20 December 2016; Published: 24 December 2016

Abstract: Electrical efficiency can be increased by combining photovoltaic (PV) and the thermoelectric (TE) systems. However, a simple and cursory combination is unsuitable because the negative impact of temperature on PV may be greater than its positive impact on TE. This study analyzed the primary constraint conditions based on the hybrid system model consisting of a PV and a TE generator (TEG), which includes TE material with temperature-dependent properties. The influences of the geometric size, solar irradiation and cold side temperature on the hybrid system performance is discussed based on the simulation. Furthermore, the effective range of parameters is demonstrated using the image area method, and the change trend of the area with different parameters illustrates the constraint conditions of an efficient PV-TE hybrid system. These results provide a benchmark for efficient PV-TEG design.

Keywords: PV-TEG; geometric size; electrical efficiency; cold side temperature

1. Introduction

The most common approach in the use of solar energy is to convert it into two easily harnessed forms, namely, electricity and thermal energy. Aside from photovoltaic (PV) forms, which can directly achieve electricity production, thermal energy can also be converted to electricity, and one promising method is to use a thermoelectric generator (TEG). The TEG has numerous advantages, such as gas-free emissions, solid-state operation, no chemical reactions, vast scalability, a long lifetime of reliable and maintenance-free operation without any moving parts and environmental damage [1,2]. Furthermore, PV can directly convert the solar radiation near the ban gap to electricity, and the infrared energy is utilized by the TEG to convert the heat to electricity. Thus, combining PV with TEG can fully utilize the solar spectrum.

PV-TE systems have been given considerable attention. Van Sark estimated PV-TE hybrid efficiency up to 23% based on poly-Si. However, heat losses and reflection were ignored during the research process [3]. Dallan et al. reported that the TEG can boost the power generation of the PV up to 39% [4]. Wang et al. illustrated that the efficiency of a DSSC/TEG hybrid system with and without SSA is 13.8% and 12.8%, respectively [5]. Beeri et al. indicated that the hybrid CPV-TE system has a potential to have more than 50% conversion efficiency with more advances in CPV cells and thermoelectric materials [6]. Rezania and Rosendahl analysed the feasibility of this and conducted a parametric evaluation of the hybrid concentrated photovoltaic-thermoelectric system [7].

Ravita and Kaushik analysed the performance of the concentrated PV-TE hybrid power generation system based on a theoretical model [8]. A theoretical model for evaluating the efficiency of the concentrating PV-PCM-TE system has been introduced by Cui et al, meanwhile, the feasibility of the system with four types of PV cells—c-Si, CIGS, single-junction GaAs, and GaInP/InGaAs/Ge (III–V)—were investigated respectively [9]. Liao et al studied the effect of solar radiation, concentration ratio and ZT among others on PV-TE based on a theoretical model [10]. Xu et al. combined light-trapping and anti-reflection in a PV-TE system and established photon management in full spectrum (300–2500 nm) [11]. Su et al. built a thermal and electric model based on two existing models of the DSSC and semiconductor TEG. A temperature coefficient was introduced to determine the DSSC electrical performance [12]. Ju et al. simulated and optimized a spectrum splitting concentration PV-TE [13]. Wu et al. discussed the performance of the PV-TE system with and without glass cover, and the external factors that affect system behaviour were analysed [14]. Li et al. illustrated a novel PV-TE with a plane heat pipe and conducted a preliminary economic analysis [15].

The theory and technology of PV-TEG have been also discussed and extensively developed in these articles [16–20]. Kossyvakis et al. conducted an experimental analysis of a tandem PV-TE hybrid system, and the experimental results showed that the corresponding improvement in maximum temperature was up to 22.5% and 30.2% for the poly-Si and the dye-sensitized based configurations, respectively [16]. Zhang and Xuan increased the solar energy utilization efficiency of the PV-TE system by developing an efficient photon management method [17]. The load matching of a PV-TE hybrid system was analysed by Lin et al. [18] and Park et al. [19]. Hashim et al. studied the geometry optimisation model of thermoelectric devices in a hybrid PV-TE system, and reported that the trade-off between the large power output and the minimum consumption of thermoelectric materials also needs to be considered in geometry optimisation [20].

Previous studies have focused mostly on the advantages of the PV-TE, however, in many cases, the electrical efficiency of PV-TE is lower than that of conventional PVs because of the negative effect of temperature on PV. In addition, the different thermal conductivities of the materials lead to different temperature distributions in the thermoelements, but, in most studies, the thermal conductivity, the electric conductivity and the Seebeck coefficient are simplified as constants. Given the temperature dependence of thermal conductivity, the electric conductivity and the Seebeck coefficient, the power factor of the n- and p-type elements differs. Nevertheless, there are few studies that discuss the constraint conditions of an efficient PV-TE based on the temperature-dependent properties of TE material, especially examining its feasibility and establishing the ideal relationship among parameters under constraint conditions

Therefore, the temperature-dependent properties of TE materials are considered to maximise efficiency of the PV-TE hybrid system in the present study. Geometry parameters, solar irradiation and cold side temperature are analysed to illustrate PV-TE feasibility. In addition, the PV-TE constraint conditions with higher electrical efficiency than the conventional PV are discussed. The feasible parameter scopes are also displayed in the images. These results can serve as a reference for PV-TE system design.

2. Model Description of a Hybrid PV-TE System

The simulated PV-TEG system consists of a solar concentrator, a tedlar layer, and a heat sink, as well as a PV and a TEG module as shown in Figure 1. The solar irradiation passes through the solar concentrator, and then one portion of the solar energy is converted to PV electricity; another portion is lost to the environment by radiation and convection, and the remaining heat is transferred to the TEG module through heat conduction. At last, a portion of the thermal energy absorbed by the TEG module is converted to electricity with the Seebeck effect [21] and most of the heat is taken away by the heat sink. The two subsystems (PV module and TEG module) are analyzed and discussed in sequence to clarify the working process of the PV-TEG hybrid system.

The following assumptions are made:

- The temperature of the PV module and heat sink module is uniform.
- Heat is transferred in only one dimension.

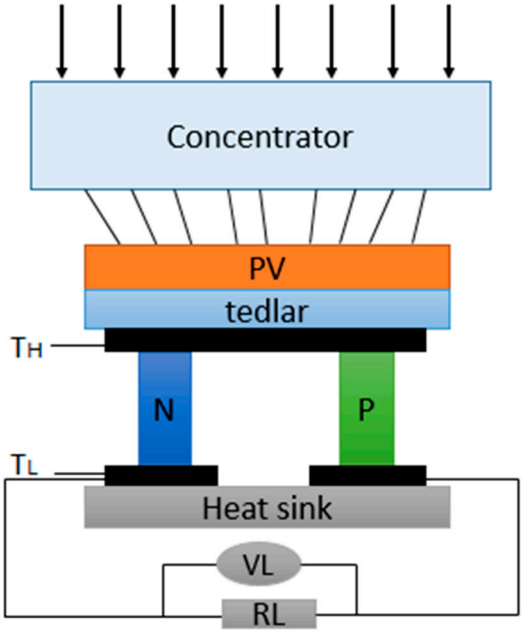

Figure 1. Schematic diagram of the PV-TEG hybrid system.

All the parameters are presented in Table 1.

Table 1. Parameters used in PV-TEG system mode.

Parameters	Symbol	Value	References
Ambient temperature	T_a	298 K	[14]
Solar irradiation	G	1000 W/m^2	-
Absorptivity of PV module	α_c	0.9	[14]
Thickness of PV	L_c	0.0003 m	[14]
Thickness of tedlar	L_T	0.000175 m	[14]
Conductivity of PV	K_c	148 W/(mK)	[14]
Conductivity of tedlar	K_T	0.2 W/(mK)	[14]
Emissivity of PV	ε_c	0.88	[22]
Temperature coefficient	φ_c	0.004 K^{-1}	[23,24]
Area of PV	A_c	0.0001 m^2	-
PV efficiency at standard condition	η_c	0.15	[24]

2.1. PV Module

The solar irradiation is concentrated on the PV module through the solar concentrator, and the energy balance equation can be expressed as:

$$CGA_c\alpha_c = E_{pv} + (h_{wind} + h_{r,c-a})(T_c - T_a)A_c + Q_H \quad (1)$$

h_{wind} and $h_{r,c-a}$ are the corresponding coefficients on the outer surface which can be expressed as [25]:

$$h_{wind} = 2.8 + u_w \quad (2)$$

$$h_{r,c-a} = \varepsilon_c \sigma ({T_c}^2 + {T_a}^2)(T_c + T_a) \tag{3}$$

where u_w is the environmental wind velocity, ε_c is the emissivity of PV, and σ is the Stefan-Boltzmann's constant.

E_{pv} can be expressed as a function of solar irradiation and temperature, shown as [26]

$$E_{pv} = CGA_c\eta_c[1 - \varphi_c(T_c - 298)] \tag{4}$$

Considering the thermal resistance in the PV module and the tedlar, then Q_H is expressed as [14]

$$Q_H = (\mathrm{T}_c - \mathrm{T}_H)(\frac{L_c}{k_c} + \frac{L_T}{k_T})^{-1} A_c \tag{5}$$

where k_c and k_T are the thermal conductivity of the PV and the tedlar, respectively. L_c and L_T are their corresponding thicknesses.

2.2. TEG Module

Based on the Seebeck effects of the thermoelectric materials, the heat input Q_H from the solar concentrator and the heat rejection Q_L from the TEG to the heat sink can be shown as [27],

$$Q_H = SI_{TE}T_H - 0.5{I_{TE}}^2R + K(T_H - T_L) \tag{6}$$

$$Q_L = SI_{TE}T_L + 0.5{I_{TE}}^2R + K(T_H - T_L) \tag{7}$$

I_{TE} is the current and can be expressed as:

$$I_{TE} = \frac{S(T_H - T_L)}{R + R_l} \tag{8}$$

The internal resistance can be expressed as:

$$R = R_n + R_p = [(\sigma_n \frac{A_n}{H_n})^{-1} + (\sigma_p \frac{A_p}{H_p})^{-1}] \tag{9}$$

where A_n and A_p are the cross-sectional areas of the *p*- and *n*- type elements, respectively. H_n and H_p are the height of the p- and n- type elements, respectively.

When the internal resistance is equal to the load resistance, the output of TEG can attain the maximum value. The relationship between the thermal conductivity, the electric conductivity, the Seebeck coefficient and the temperature is shown in Figure 2 [28]. The values of these parameters with different temperatures can then be obtained.

The output energy of PV is:

$$P_{TEG} = Q_H - Q_L \tag{10}$$

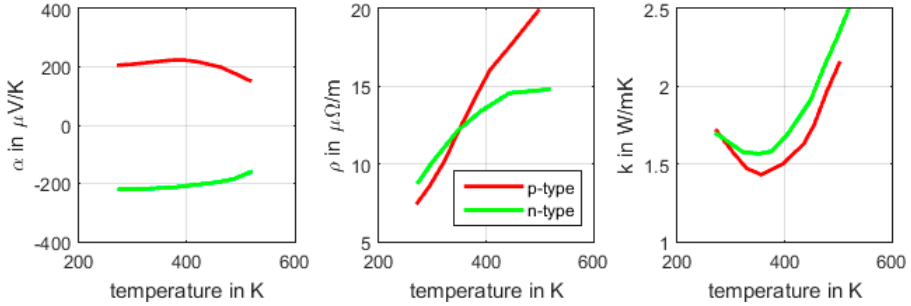

Figure 2. Thermoelectric characteristics of Bi_2Te_3.

2.3. Overall Electrical Output and Efficiency of PV-TEG System

The total electricity production P is the sum of PV module and TEG module electrical outputs,

$$P = P_{pv} + P_{TEG} = E_{pv} + P_{TEG} \tag{11}$$

and the overall efficiency of the PV-TEG system is:

$$\eta = \frac{E_{pv} + P_{TEG}}{CGA_c} \tag{12}$$

3. Analysis and Optimization of the Hybrid System's Performance

The performance of the hybrid PV-TE system depends on a series of physical parameters such as the height H, the cross-sectional area S of TEG, the solar irradiation G, cold side temperature T_L, the ambient temperature T_a, the area of PV A_c and the electrical current I_{TE}. This paper analyzes the effect of the series of parameters on the performance of the hybrid system, and optimizes them under different conditions.

3.1. Geometric Parameters of TEG

The relationship curve between the TEG's height and the overall efficiency is shown in Figure 3, where G = 1000 W/m^2, C = 5, T_L = 273.15 K, and the TEG height range from 1 mm to 31 mm. Furthermore, the cross-sectional area is a set of five different values, i.e., S = 1 mm^2, S = 10 mm^2, S = 20 mm^2, S = 30 mm^2 and S = 40 mm^2. It can be seen that the overall efficiency of the hybrid system decreases as the TEG height increases, and the overall efficiency η will be lower than 15% when the height is more than 30 mm which indicates that these sizes are unsuitable under these conditions. Moreover, the result shows that the hybrid system can yield a higher overall efficiency when S increases to the same TEG height. In addition, Figure 3 shows that overall efficiency is always lower than 15% when S is 1 mm^2. Evidently, it can be concluded that the overall efficiency will exceed 15% when H is small and S is large which is appropriate to the conditions of the PV-TEG system instead of the PV system. It can also be seen that the overall efficiency increases as the cross-section areas enlarge. The lower TEG height responds to the higher overall electrical efficiency within the same cross-sectional area.

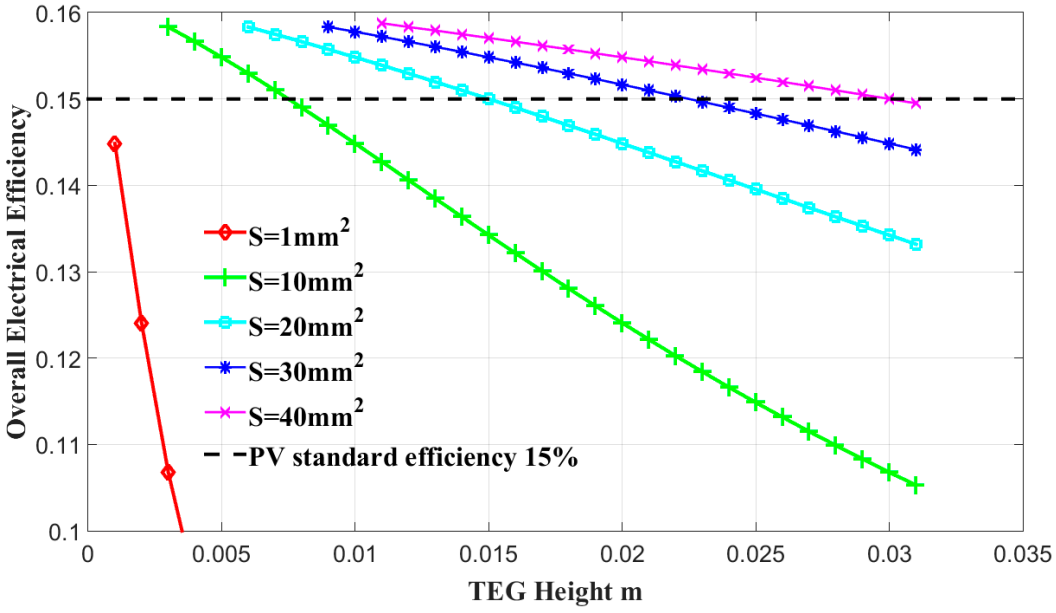

Figure 3. The curves of the overall efficiency η with different TEG heights H.

As shown in Figure 4, the yellow region indicates that the overall efficiency is greater than 15% while the remaining area shows an overall efficiency lower than 15%. It can be seen that when the parameters (height and cross sectional area) of the PV-TEG hybrid system are located in the yellow region, the design is appropriate. Furthermore, the left border of the yellow region represents the curve of the maximum efficiency at the same cross sectional area, while the right border indicates the curve of the overall efficiency is 15%. The maximum efficiency is 15.89% (red point) when the height is 11.6 mm and the cross-sectional area is 45.5 mm^2. The linear fitting of the two border curves is shown in Figure 5. The expression of the maximum efficiency fitting curve is:

$$H_1 = 270S - 0.00011 \tag{13}$$

On the other hand, the variation of the height H with the cross-sectional area S is the linear relationship when H and S satisfy an overall efficiency of 15%:

$$H_2 = 750S - 0.00048 \tag{14}$$

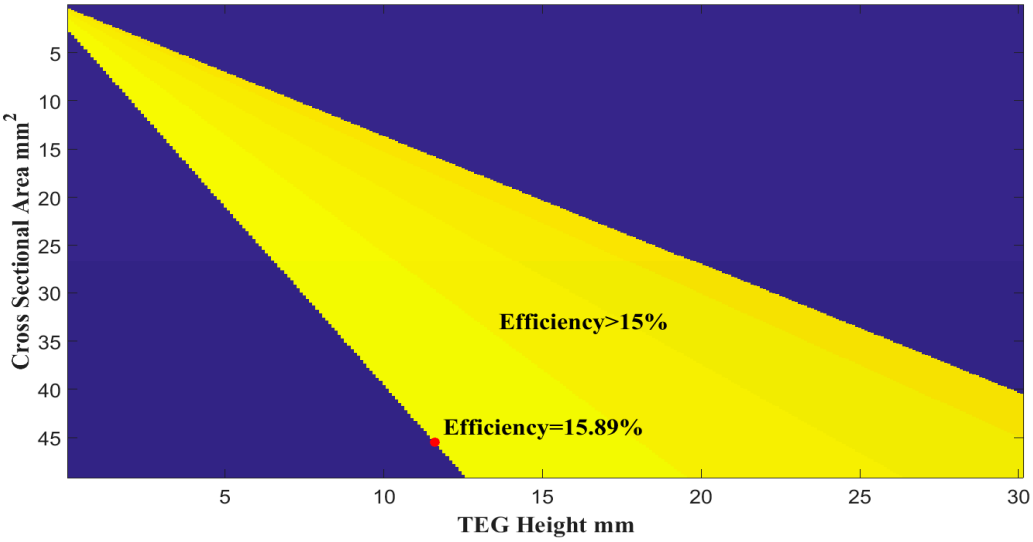

Figure 4. Corresponding relationship between the TEG height and the cross sectional area with optical concentration ratio of 5X.

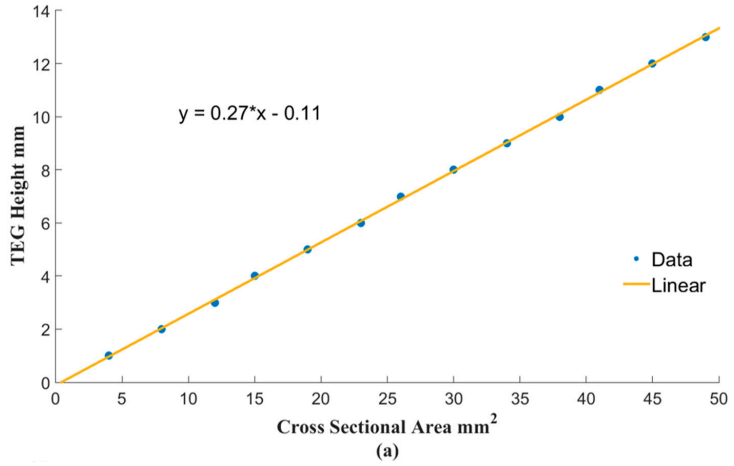

Figure 5. *Cont.*

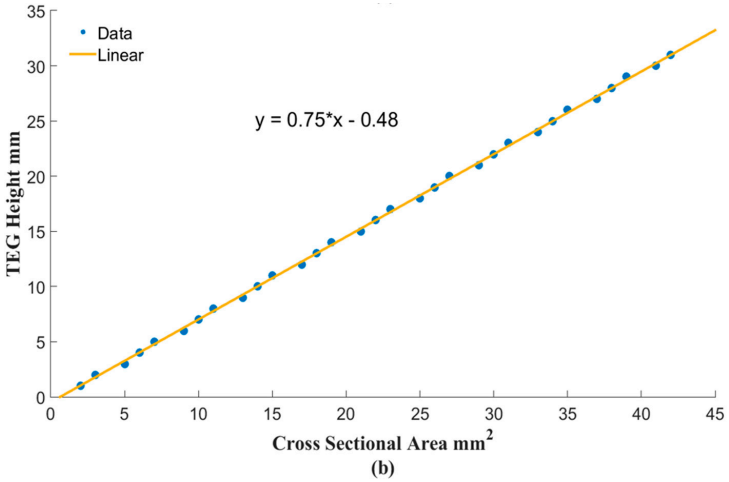

Figure 5. Fitting of the yellow scope border, (**a**) maximum efficiency fitting curve; (**b**) relationship between the height and the cross-sectional area with an overall efficiency of 15%.

3.2. Solar Irradiation

The variation curve of the overall efficiency is shown in Figure 6a, where the optical concentration ratio ranges from 1 to 20 and the cross-section area is set for five different values, i.e., $S = 10$ mm^2, $S = 15$ mm^2, $S = 20$ mm^2, $S = 25$ mm^2 and $S = 30$ mm^2. As shown in Figure 6b, the TEG height is also set for five different values, i.e., $H = 10$ mm, $H = 15$ mm, $H = 20$ mm, $H = 25$ mm and $H = 30$ mm. A larger optical concentration ratio responds to the lower performance of the hybrid PV-TEG system. Thus, the PV-TEG system along with these structures are not optimal when the optical concentration ratio is large since the overall efficiency is lower than 15%. In addition, the overall efficiency will increase when the cross-sectional area S increases or the height H decreases.

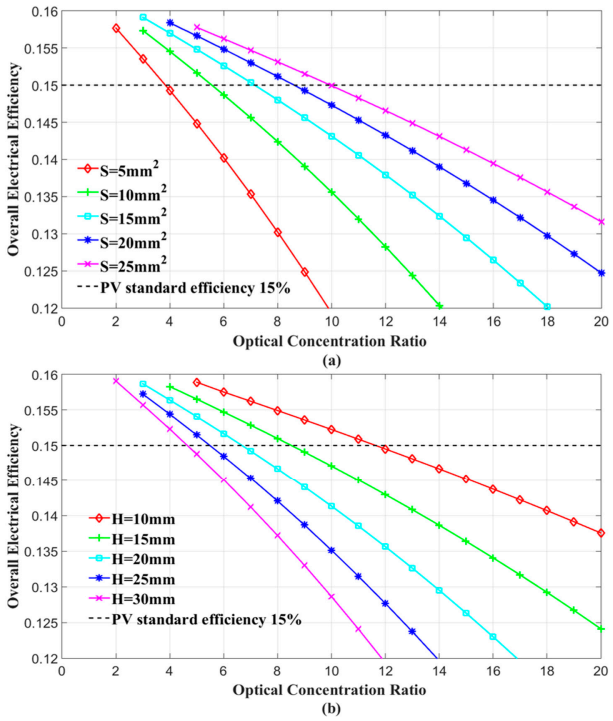

Figure 6. The curves of the overall efficiency η with the different solar irradiation values G, (**a**) different cross-section areas; (**b**) different heights.

As seen from Figure 7, the yellow area becomes smaller as the height increases. This means that the constraint conditions of an efficient PV-TE hybrid system become stricter as the height increases. Furthermore, the cross-sectional area becomes larger and the optical concentration ratio becomes smaller within the height increases.

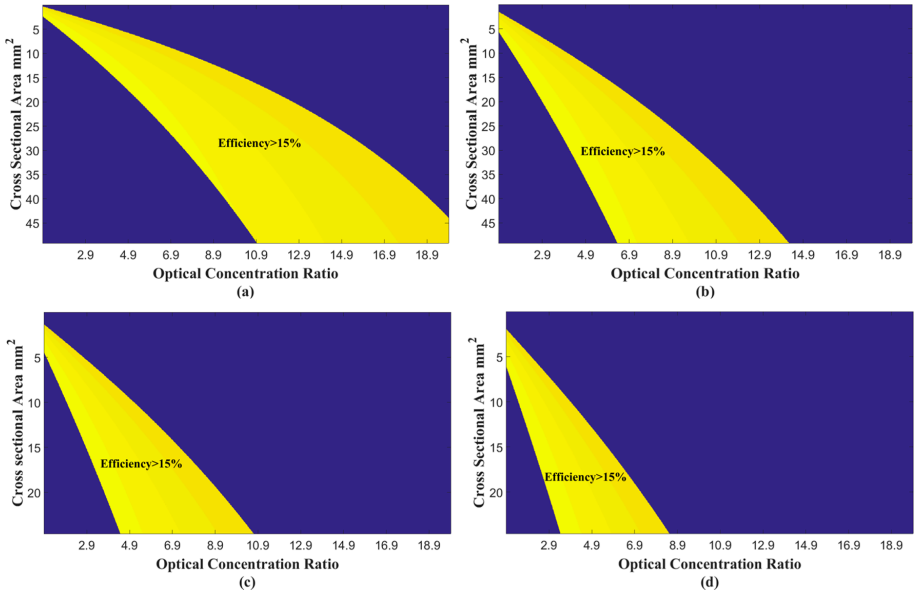

Figure 7. Corresponding relationship between the optical concentration ratio and the cross-sectional area with (**a**) H = 5 mm (**b**) H = 10 mm (**c**) H = 15 mm (**d**) H = 20 mm.

Contrary to Figure 7, Figure 8 illustrates that the yellow area becomes larger as the cross-sectional area increases. This indicates that the constraint conditions of an efficient PV-TE hybrid system become less strict as the cross-sectional area increases. In addition, the height and the optical concentration ratio becomes larger when the cross-sectional area increases.

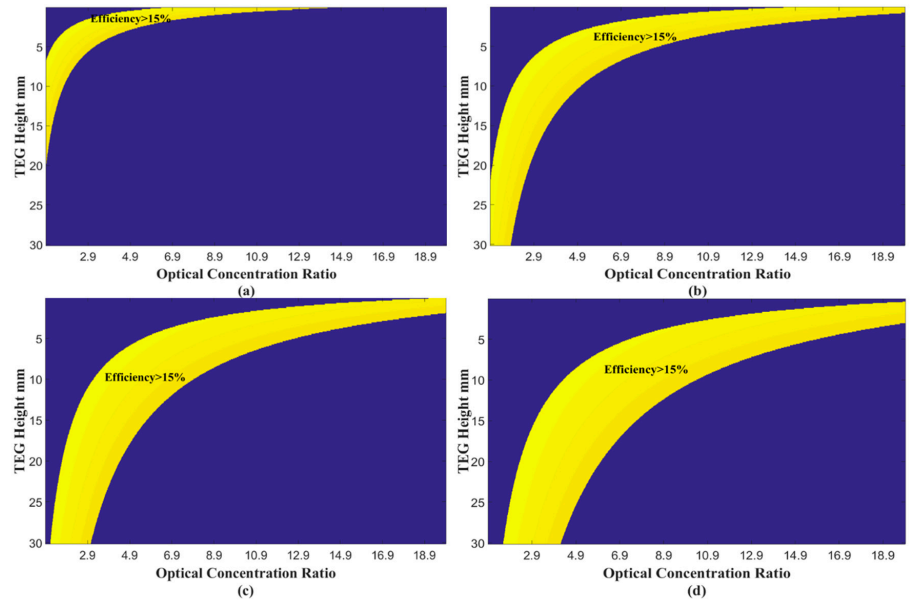

Figure 8. Corresponding relationship between the optical concentration ratio and the TEG height with (**a**) S = 5 mm^{-2} (**b**) S = 15 mm^{-2} (**c**) S = 25 mm^{-2} (**d**) S = 35 mm^{-2}.

3.3. Cold Side Temperature

It can be seen from Figure 9 that the overall efficiency decreases when the cold side temperature increases and the optical concentration ratio is 5 and the ambient temperature is 298 K. For example, the overall efficiency with S = 25 mm^2 will be lower than 15% when the temperature is higher than approximately 285 K. Figure 9a,b shows that the overall efficiency will increase when the cross-sectional area increases or the height decrease.s When the cold side temperature is high, the overall electrical efficiency of the PV-TEG hybrid system is lower than 15.0%, which corresponds to the PV system. Thus, the low cold side temperature is a precondition for a high-efficiency PV-TEG system.

Figure 10 demonstrates that the yellow area becomes larger and then smaller as the height increases. For the low height, efficient coupling responds to the low cold side temperature and the low cross-sectional area.

As the cross-sectional area increases, the yellow area becomes larger (Figure 11). This finding indicates that the constraint conditions of an efficient PV-TE hybrid system are less strict as the cross-sectional area increases. However, the TEG height is usually low and the cross-sectional area is small because of costs in actual application, which increases the complexity of parameter coupling.

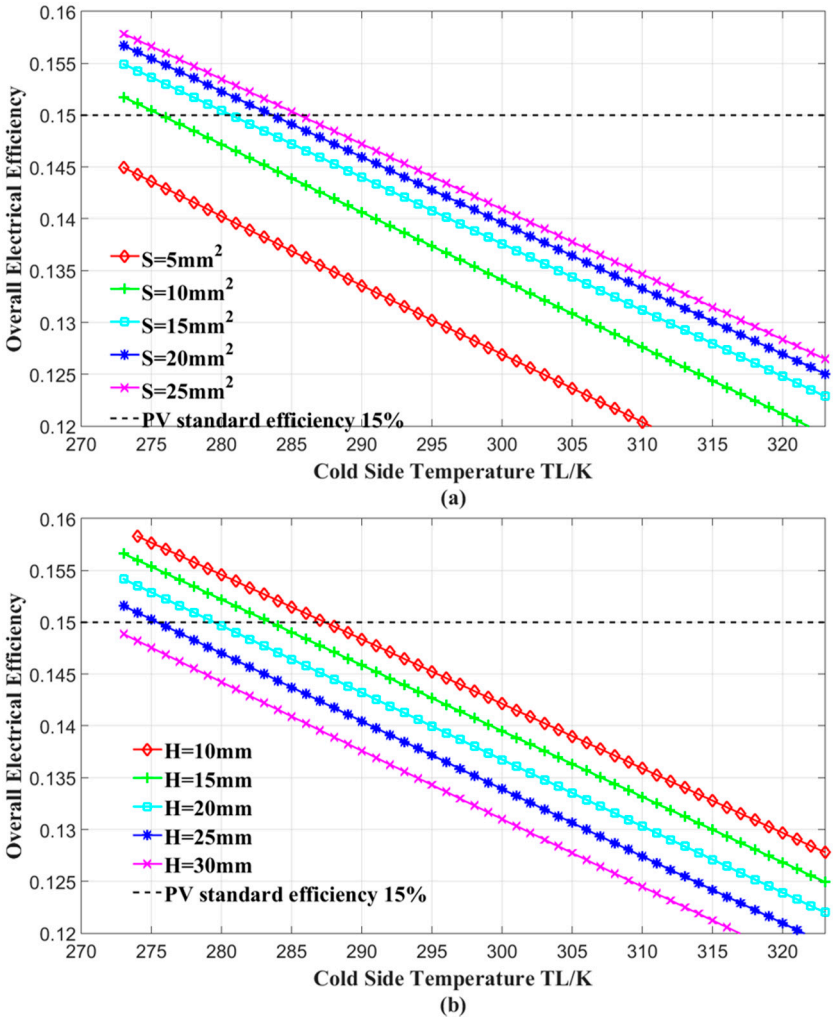

Figure 9. The curves of the overall efficiency η with the different cold temperatures T_L, (**a**) different cross-section areas; (**b**) different heights.

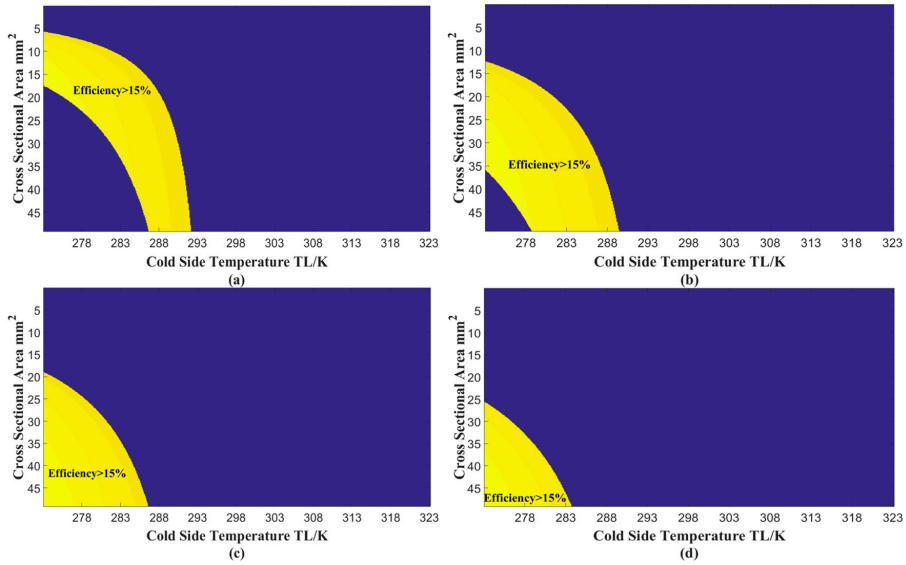

Figure 10. Corresponding relationship between the cold side temperature and the cross-sectional area with (**a**) H = 5 mm (**b**) H = 10 mm (**c**) H = 15 mm (**d**) H = 20 mm.

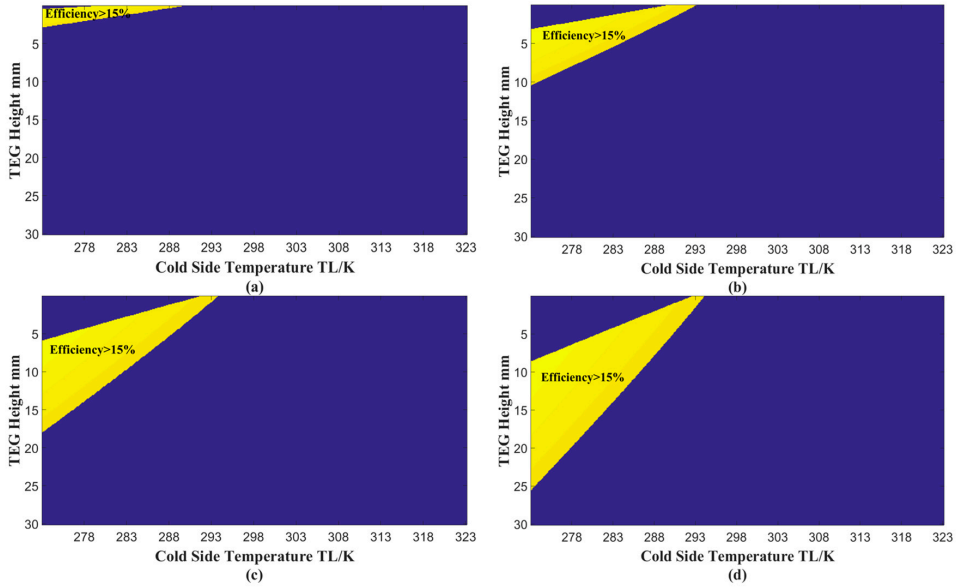

Figure 11. Corresponding relationship between the cold side temperature and the TEG height with (**a**) S = 5 mm^{-2} (**b**) S = 15 mm^{-2} (**c**) S = 25 mm^{-2} (**d**) S = 35 mm^{-2}.

4. Conclusions

In this study, a PV-TEG hybrid system is established based on the temperature-dependent properties of TE materials. The impact of the TEG height and cross-sectional area, the solar irradiation and the cold side temperature on the overall efficiency is analyzed. A demonstration of the PV-TEG hybrid system is carried out to show that the height and the cross-sectional area of TEG have an approximately linear relationship with the overall efficiency of maximum output. The primary constraint conditions of an efficient PV-TE hybrid system can be summarized as follows:

The overall efficiency is higher with a larger cross-sectional area and the height of TEG is lower when the optical concentration ratio or the cold side temperature is constant.

The overall efficiency is maximised when the height and cross-sectional area of TEG satisfy the following formula: $H_1 = 270S - 0.00011$. The variation in height with the cross-sectional area is linear when H and S satisfy an overall efficiency of 15%: $H_2 = 750S - 0.00048$.

The effective range of parameters is shown using the image area method, and the change trend of the area with different parameters is indicated to reflect the constraint conditions of an efficient PV-TE hybrid system. The constraint conditions of an efficient PV-TE hybrid system are less strict as the cross-sectional area increases. However, the TEG height is usually low and the cross-sectional area is small because of costs in actual application, which will increase the complexity of parameter coupling.

Acknowledgments: The study was sponsored by the National Science Foundation of China (Grant Nos. 51408578, 51611130195), Anhui Provincial Natural Science Foundation (1508085QE96).

Author Contributions: The idea was proposed by Guiqiang Li, who was responsible for writing the paper. Xiao Chen carried out the calculation. Yi Jin improved this paper.

Conflicts of Interest: The authors declare no conflict of interest.

Nomenclature

A	area, m^2	T_C	PV temperature, K
C	Concentration ratio	T_H	hot side temperature of TE, K
E_{pv}	electricity generation of PV module, W	T_L	cold side temperature of TE, K
G	solar radiation obtained by the solar concentrator W/m^2	***Greek Symbols***	
$h_{r,c-a}$	radiation heat transfer coefficient on outer surface, $W/(m^2K)$	α	absorptivity
h_{wind}	convection heat transfer coefficient on outer surface, $W/(m^2K)$	β_c	packing factor
I_{TE}	operating current, A	φ	solar cell temperature coefficient, K^{-1}
k	thermal conductivity, $W/(mK)$	η	efficiency
K	total thermal conductance of a TE module, W/K	ε	emissivity
L	thickness, m	σ	electric conductivity
P	electricity outputs, W	***Subscripts***	
Q	heat conducted in thermoelectric modules, W	a	air
R	total electrical resistance of a TE module, Ω	n	n-type
R_l	load resistance, Ω	p	p-type
u_w	wind velocity, m/s	pv	PV module
S	total Seebeck coefficient of a TE module, V/K	TE	the TEG module

References

1. Li, G.Q.; Ji, J.; Zhang, G.; He, W.; Chen, X.; Chen, H.B. Performance analysis on a novel micro-channel heat pipe evacuated tube solar collector-incorporated thermoelectric generation. *Int. J. Energy Res.* **2016**, *40*, 2117–2127. [CrossRef]
2. Li, G.Q.; Zhang, G.; He, W.; Ji, J.; Lv, S.; Chen, X.; Chen, H.B. Performance analysis on a solar concentrating thermoelectric generator using the micro-channel heat pipe array. *Energy Convers. Manag.* **2016**, *112*, 191–198. [CrossRef]
3. Van Sark, W. Feasibility of photovoltaic thermoelectric hybrid modules. *Appl. Energy* **2011**, *88*, 2785–2790. [CrossRef]
4. Dallan, B.S.; Schumann, J.; Lesage, F.J. Performance evaluation of a photoelectric-thermoelectric cogeneration hybrid system. *Sol. Energy* **2015**, *118*, 276–285. [CrossRef]
5. Wang, N.; Han, L.; He, H.; Park, N.-H.; Koumoto, K. A novel high-performance photovoltaic-thermoelectric hybrid device. *Energy Environ. Sci.* **2011**, *4*, 3676–3679. [CrossRef]
6. Beeri, O.; Rotem, O.; Hazan, E.; Katz, E.A.; Braun, A.; Gelbstein, Y. Hybrid photovoltaic thermoelectric system for concentrated solar energy conversion: Experimental realization and modeling. *J. Appl. Phys.* **2015**, *118*. [CrossRef]

7. Rezania, A.; Rosendahl, L.A. Feasibility and parametric evaluation of hybrid concentrated photovoltaic-thermoelectric system. *Appl. Energy* **2017**, *187*, 380–389. [CrossRef]
8. Lamba, R.; Kaushik, S.C. Modeling and performance analysis of a concentrated photovoltaic-thermoelectric hybrid power generation system. *Energy Convers. Manag.* **2016**, *115*, 288–298. [CrossRef]
9. Cui, T.F.; Xuan, Y.M.; Li, Q. Design of a novel concentrating photovoltaic-thermoelectric system incorporated with phase change materials. *Energy Convers. Manag.* **2016**, *112*, 49–60. [CrossRef]
10. Liao, T.J.; Lin, B.H.; Yang, Z.M. Performance characteristics of a low concentrated photovoltaic-thermoelectric hybrid power generation device. *Int. J. Therm. Sci.* **2014**, *77*, 158–164. [CrossRef]
11. Xu, Y.P.; Xuan, Y.M.; Yang, L.L. Full-spectrum photon management of solar cell structures for photovoltaic-thermoelectric hybrid systems. *Energy Convers. Manag.* **2015**, *103*, 533–541. [CrossRef]
12. Su, S.H.; Liu, T.; Wang, Y.; Chen, X.H.; Wang, J.T.; Chen, J.C. Performance optimization analyses and parametric design criteria of a dye-sensitized solar cell thermoelectric hybrid device. *Appl. Energy* **2014**, *120*, 16–22. [CrossRef]
13. Ju, X.; Wang, Z.F.; Flamant, G.; Li, P.; Zhao, W.Y. Numerical analysis and optimization of a spectrum splitting concentration photovoltaic-thermoelectric hybrid system. *Sol. Energy* **2012**, *86*, 1941–1954. [CrossRef]
14. Wu, Y.-Y.; Wu, S.-Y.; Xiao, L. Performance analysis of photovoltaic-thermoelectric hybrid system with and without glass cover. *Energy Convers. Manag.* **2015**, *93*, 151–159. [CrossRef]
15. Li, G.Q.; Zhao, X.D.; Ji, J. Conceptual development of a novel photovoltaic-thermoelectric system and preliminary economic analysis. *Energy Convers. Manag.* **2016**, *126*, 935–943. [CrossRef]
16. Kossyvakis, D.N.; Voutsinas, G.D.; Hristoforou, E.V. Experimental analysis and performance evaluation of a tandem photovoltaic-thermoelectric hybrid system. *Energy Convers. Manag.* **2016**, *117*, 490–500. [CrossRef]
17. Zhang, Y.T.; Xuan, Y.M. Biomimetic omnidirectional broadband structured surface for photon management in photovoltaic-thermoelectric hybrid systems. *Sol. Energy Mater. Sol. Cells* **2016**, *144*, 68–77. [CrossRef]
18. Lin, J.; Liao, T.J.; Lin, B.H. Performance analysis and load matching of a photovoltaic-thermoelectric hybrid system. *Energy Convers. Manag.* **2015**, *105*, 891–899. [CrossRef]
19. Park, K.-T.; Shin, S.-M.; Tazebay, A.S.; Um, H.-D.; Jung, J.-Y.; Jee, S.-W.; Oh, M.-W.; Park, S.-D.; Yoo, B.Y.; Yu, C.; et al. Lossless hybridization between photovoltaic and thermoelectric devices. *Sci. Rep.* **2013**, *3*. [CrossRef] [PubMed]
20. Hashim, H.; Bomphrey, J.J.; Min, G. Model for geometry optimisation of thermoelectric devices in a hybrid PV/TE system. *Renew. Energy* **2016**, *87*, 458–463. [CrossRef]
21. Jaworski, M.; Bednarczyk, M.; Czachor, M. Experimental investigation of thermoelectric generator (TEG) with PCM module. *Appl. Therm. Eng.* **2016**, *96*, 527–533. [CrossRef]
22. Najafi, H.; Woodbury, K.A. Modeling and analysis of a combined photovoltaic-thermoelectric power generation system. *J. Sol. Energy Eng.* **2013**, *135*, 1–8. [CrossRef]
23. Li, G.Q.; Pei, G.; Ji, J.; Su, Y.H. Outdoor overall performance of a novel air-gap-lens-walled compound parabolic concentrator (ALCPC) incorporated with photovoltaic/thermal system. *Appl. Energy* **2015**, *144*, 214–223. [CrossRef]
24. Li, G.Q.; Pei, G.; Ji, J.; Yang, M.; Su, Y.H.; Xu, N. Numerical and experimental study on a PV/T system with static miniature solar concentrator. *Sol. Energy* **2015**, *120*, 565–574. [CrossRef]
25. Watmuff, J.H.; Charters, W.W.S.; Proctor, D. Solar and wind induced external coefficients—Solar collectors. *Complex* **1977**, *2*, 56.
26. Chow, T.T.; He, W.; Ji, J. Hybrid photovoltaic-thermosyphon water heating system for residential application. *Sol. Energy* **2006**, *80*, 298–306. [CrossRef]
27. Ding, L.C.; Akbarzadeh, A.; Date, A. Performance and reliability of commercially available thermoelectric cells for power generation. *Appl. Therm. Eng.* **2016**, *102*, 548–556. [CrossRef]
28. Gao, J.-L.; Du, Q.-G.; Zhang, X.-D.; Jiang, X.-Q. Thermal Stress Analysis and Structure Parameter Selection for a Bi2Te3-Based Thermoelectric Module. *J. Electron. Mater.* **2011**, *40*, 884–888. [CrossRef]